

Suitability of infrared spectroscopic imaging as an intraoperative tool in cerebral glioma surgery

Stephan B. Sobottka · Kathrin D. Geiger ·
Reiner Salzer · Gabriele Schackert · Christoph Krafft

Received: 20 June 2008 / Revised: 25 September 2008 / Accepted: 26 September 2008 / Published online: 16 October 2008
© Springer-Verlag 2008

Abstract Infrared spectroscopic imaging is a promising intraoperative tool which enables rapid, on-site diagnosis of brain tumors during neurosurgery. A classification model was recently developed using infrared spectroscopic images from thin tissue sections to grade malignant gliomas, the most frequent class of primary brain tumor. In this study the model was applied to 54 specimens from six patients with inhomogeneous gliomas composed of regions with different tumor density and morphology. The resection was controlled using neuronavigation which transfers the findings obtained by preoperative magnetic resonance imaging (MRI) into the operating field. For comparison, all specimens were independently evaluated by histopathology after hematoxylin and eosin staining. The infrared-derived grading agreed with histopathology and MRI findings for almost all specimens. With regard to histopathological assessment, sensitivities of 100% (22/22) and 93.1% (27/29) and specificities of 96.9%

(31/32) and 88.0% (22/25) were achieved, depending on whether the classification was based on the predominant or maximal tumor grade, respectively, in the specimen. Altogether, in 98% (53/54) of all specimens the decision to continue or not continue tumor resection could have been made according to the infrared spectroscopic classification. This retrospective study clearly demonstrates that infrared spectroscopic imaging may help to define tumor margins intraoperatively and to detect high-grade tumor residues for achieving more radical tumor resection.

Keywords FTIR imaging · Neurosurgery · Neuropathology · Magnetic resonance imaging

Introduction

Malignant gliomas are the most frequent primary brain tumors. Tumor resection is usually the first treatment of choice to achieve the most favorable condition for further adjuvant therapeutic modalities such as radiotherapy, chemotherapy, or experimental therapeutic options. In this respect surgery has to fulfill essentially two different tasks: first, to diagnose the glioma and to classify the tumor according to the World Health Organization (WHO) classification system, and, second, to achieve the most radical removal of the contrast-enhancing tumor portion which represents high-grade glioma tissue. There is growing evidence that the extent of resection affects the overall survival of patients [1–7]. However, complete resection of the contrast-enhanced portion of the tumor is achieved in less than 40% of cases, due to the uncertainty involved in identifying viable tumor margins during surgery [7].

To achieve more complete tumor resection, multiple snap-frozen tissue sections of suspicious specimens may be

S. B. Sobottka · G. Schackert
Department of Neurosurgery, University Hospital,
Dresden University of Technology,
Fetscherstr. 74,
01307 Dresden, Germany

K. D. Geiger
Department of Neuropathology, Institute for Pathology,
University Hospital, Dresden University of Technology,
Fetscherstr. 74,
01307 Dresden, Germany

R. Salzer · C. Krafft
Bioanalytical Chemistry, Dresden University of Technology,
01062 Dresden, Germany

C. Krafft (✉)
Institute of Photonic Technology,
Albert-Einstein-Str. 9,
07745 Jena, Germany
e-mail: christoph.krafft@ipht-jena.de

intraoperatively assessed by a neuropathologist. The problems are that such an expert is not always available and the quality and quantity of the tissue sample are sometimes not sufficient for accurate diagnosis. In addition, the following concepts have been introduced to the clinical setting:

- First, imaging techniques such as frameless stereotactic navigation (neuronavigation) or intraoperative magnetic resonance imaging (MRI) have been used to improve the extent of tumor resection [8–10]. Both methods enable excellent visualization of eloquent neural structures that need to be preserved during surgery. However, extensive costs limit the availability of intraoperative MRI. The occurrence of brain shift during surgical intervention affects accuracy in defining exact tumor borders using neuronavigation based on preoperative MRI information.
- Second, fluorescence-guided resection of high-grade glioma uses 5-aminolevulinic acid (5-ALA) as contrast agent. Following administration of 5-ALA fluorescent porphyrins accumulate in malignant glioma tissue and can be visualized intraoperatively by use of a modified neurosurgical microscope [7]. This approach is limited by the photostability and uptake of the contrast agent.

As an adjunct to histopathology, infrared (IR) spectroscopic imaging showed high potential for a rapid and semi-automated diagnosis of human brain tumors. One of the main advantages is that IR spectroscopy provides detailed molecular information without labels such as contrast enhancing agents or stains. Whereas the first is used for fluorescence spectroscopy and MRI, the latter is used for histopathology. Another advantage is that the spectroscopic information can be combined with lateral resolution on the single-cell level using the rapid imaging spectrometers which have become commercially available in recent years. These spectrometers utilize the multiplex advantage of the Fourier-transform technique and the multichannel advantage of focal plane array detectors. The application of IR spectroscopy in the context of brain tumor surgery has recently been summarized [11]. In particular, human brain tissue, brain tumors, and tumor cells were analyzed by IR spectroscopy [12]; by use of different techniques of chemometric image processing, diagnosis and classification of gliomas according to the WHO grading system were performed with accuracy of up to 90% [13, 14]. The primary tumors were identified for human brain metastases [15, 16]. Raman spectroscopy is a related technique which also probes molecular vibrations as a fingerprint for tissue. A good correlation between IR and Raman spectroscopy was found for tissue sections of human intracranial tumors [17]. Raman spectra were also collected from non-dried, native specimens of brain tumors [18]. A Raman spectrometer was coupled to a fiber-optic probe to detect metastases in mouse brains [19]. This setup will

enable application of the technique under in-vivo conditions in the future.

Here, we describe, for the first time, a diagnostic classification system based on comparative evaluation of FTIR imaging, histopathology, and MRI in malignant gliomas of six patients. Tissue sections were prepared from 54 specimens from six patients with inhomogeneous gliomas composed of regions with different tumor density and morphology which were graded analogously with the WHO classification. The resection of each specimen was controlled by neuronavigation surveillance. IR spectroscopic images were collected from each tissue section and analyzed by a recently developed classification model [20, 21]. The classification results were compared with the neuropathologic evaluation. The prospects of achieving intraoperative glioma grading by IR spectroscopic analysis of multiple frozen section tissue is discussed.

Methods

Patients, tumor biopsies, and sample preparation

Six high-grade glioma patients were treated by open surgery with gross tumor removal (1 × astrocytoma WHO III, 1 × oligoastrocytoma WHO III, 1 × oligodendroglioma WHO III, 3 × glioblastoma multiforme WHO IV). Preoperative gadolinium-enhanced T1-weighted MRI scans with 2-mm slices were performed the day before surgery (Magnetom Avanto, 1.5T, Siemens, Germany). MRI were transferred to the neuronavigation system BrainLAB VectorVision (BrainLAB, Munich, Germany), a frameless image-guided surgery system that uses passive reflection of infrared flashes from reflective spheres adapted to fit surgical instruments, which are detected and tracked by a camera digitizer. All tumors were inhomogeneous and showed regions of different tumor grade, analogously with the WHO classification as indicated by MRI. Between five and twelve tissue specimens were collected during surgery and the location of the resection was stored by the neuronavigation system. Patient details (sex, age, tumor localization) are summarized in Table 1. All 54 tissue probes were snap-frozen and comparatively analyzed by IR spectroscopy and histopathological examination using consecutive sections. Serial cryosections of 5 μm thickness were mounted either on an IR-transparent calcium fluoride slide, dried in air, and imaged by IR spectroscopy in transmission mode, or on a glass slide, stained by hematoxylin and eosin (H&E), and imaged by light microscopy for histopathologic assessment by a neuropathologist without knowledge of the FTIR and MRI data. Evaluation of the morphology was carried out following the WHO classification with the most unfavorable morphology used for diagnosis in each case. However, multiple sections

Table 1 Characteristics of the six glioma patients

Patient	Sex	Age	Localization	Histology	Sample number	Contrast + (MRI)	Contrast - (MRI)
1	M	62	Left temporal	Astrocytoma °III	5	0	5
2	M	57	Right frontal	Glioblastoma °IV	12	6	6
3	F	72	Left frontal	Glioblastoma °IV	7	3	4
4	M	59	Right frontal ^a	Oligodendroglioma °III*	10	8	2
5	M	36	Right frontal	Oligoastrocytoma °III	10	7	3
6	M	63	Right temporo-polar/-occipital	Glioblastoma °IV	10	5	5

^a Local recurrent tumor

Contrast + : number of specimens showing gadolinium contrast enhancement on MRI usually representing high-grade tumor tissue

Contrast - : number of specimens showing no gadolinium contrast enhancement on MRI usually representing low-grade tumor tissue

from different tumor locations per case were also individually graded analogously with the WHO classification, regardless of the final diagnosis. In addition, normal brain tissue, hemorrhage, necrosis, or endothelial proliferation were specified separately.

IR spectroscopic imaging

IR spectroscopic images from patients 1 and 2 were recorded using an IFS66/S FTIR spectrometer coupled to a Hyperion microscope and a single-channel mercury cadmium telluride (MCT) detector (Bruker Optik, Ettlingen, Germany). Images were acquired in mapping mode using an aperture of $180 \times 180 \mu\text{m}$ and a step size of $180 \mu\text{m}$. Collecting five scans per IR spectrum at a spectral resolution of 4 cm^{-1} resulted in a scan speed of 600 spectra per hour.

IR spectroscopic images from patients 3 to 6 were recorded using an IFS66/S FTIR spectrometer coupled to the IMAC macro chamber and a 64×64 focal plane array (FPA) detector (Bruker Optik, Ettlingen, Germany). The field of view was $4 \times 4 \text{ mm}^2$ and the lateral resolution $63 \times 63 \mu\text{m}^2$ per pixel. Multiple FTIR images were recorded from tissue sections exceeding a size of $4 \times 4 \text{ mm}^2$ by moving a manual sample stage. FTIR images of 4096 IR spectra at 4 cm^{-1} spectral resolution were acquired by coaddition of 19 interferograms by the OPUS software (version 5.0, Bruker) operating the FPA in continuous-scan mode. As a consequence of the parallel acquisition, recording time was reduced to approximately 4 min per image. Ratios of the single-beam spectra of each sample FTIR image against the spectra of a background FTIR image of neat calcium fluoride slides were obtained and converted to absorbance.

Processing of FTIR images

Data processing was performed by routines written in-house in a MatLab environment (The Mathworks, Natick, MA, USA) as described previously in detail [20, 21]. Briefly, spectral backgrounds and offsets were corrected by sub-

tracting multi-point, linear baselines. IR spectra with intensities below 0.15 absorbance units were removed from the FTIR data sets because they mainly correspond to areas without tissue and have low “signal-to-noise” ratios. IR band intensities at 2850, 1655, 1545, 1450 and 1230 cm^{-1} were determined, and band ratios 2850/1655, 1545/1655, and $(1230 + 1450)/1655$ were calculated; these describe the six classes normal brain tissue, glioma °II, glioma °III, glioblastoma multiforme, hemorrhage, and other tissue. The spectral features with the highest discriminatory information were identified by comparing mean cluster spectra of FTIR images of patients 1 and 2. A subset which consists of the ratio 2850/1655 was presented in an early paper [12] to distinguish gliomas from normal brain tissue. As explained previously [20, 21] the classes of other tissue and hemorrhage would overlap with the high-grade tumor portion if the ratios 1545/1655 and $(1230 + 1450)/1655$ were excluded. In related approaches [13, 14], feature selection was part of the training process. In the context of glioblastoma multiforme (°IV), glioma °II and °III are used as descriptive terms delineating the cellularity and morphological appearance of tumor areas, analogously with the morphological parameters used for WHO grading. Based on the band ratios, the spectra were classified on one of the six classes by a linear discriminant analysis (LDA) model. The model was trained using 18 mean cluster spectra from FTIR images of patients 1 and 2 that contained each tissue type. The selected spectra defined the limits of the LDA classifiers. Although these spectra did not belong to the FTIR images of patients 1 and 2, these data were not completely independent in contrast to FTIR images of patients 3 to 6 that were even collected using different instruments. The resulting class memberships were color coded so that color-coded images could be assembled for visualization and comparison with H&E-stained parallel tissue sections. Tissue with regular cellularity was colored green, low tumor cellularity blue, intermediate tumor cellularity orange, high tumor cellularity red, hemorrhage brown, and other tissue gray. It has previously been shown

that the procedures could be applied to FTIR images that were collected using the single-channel [20] or FPA detector [21]. The spectra and the classification results did not differ significantly.

Histopathological examination

The histopathological assessment was made in a blinded fashion after classification of FTIR images was completed. After light microscopic inspection of the H&E stained tissue sections, samples were classified as regular, low tumor cellularity without anaplastic morphology, intermediate tumor cellularity, and high tumor cellularity (°I to °IV) in conjunction with histopathological criteria of the WHO glioma classification system. °IV was only assigned when endothelial proliferates and/or necroses were present in addition to a malignant morphology with high cellularity.

Comparative data analysis and evaluation

IR spectroscopic results on intraoperatively collected specimens were compared with preoperative MRI findings and postoperative histopathological evaluation. The specimens were classified as high-grade or normal to low-grade specimens with the aim of identifying the high-grade part of the tumors. The decision of whether or not to continue tumor resection was retrospectively evaluated using histopathological, IR spectroscopic, and radiological findings. FTIR images were rated using two systems—first according to the predominantly assigned class and then according to the highest grade of cellularity (worst-case evaluation). The criteria for assessment of the grade of malignancy are summarized in Table 2.

Results

Irrespective of the quality of the tissue section, all intraoperatively collected specimens could be successfully diag-

nosed by the IR spectroscopic approach in the above described technical manner. The average time for spectroscopic analysis of the snap-frozen section added up to approximately 15 min, including 10 min for preparation of the frozen section and 5 min for FTIR image acquisition using the FPA detector. Classification results were obtained almost instantaneously by using the unmanipulated FTIR images as input and executing an integrated, automatic routine. Total computing time was a few seconds depending on the performance of the computer system. As a result a colored classification map was obtained corresponding to the histological section of the biopsy specimen (Figs. 1, 2, 3).

Figure 1 gives an example of IR spectroscopic analysis of four tissue specimens from patient 2 with a right frontal inhomogeneous and contrast-enhancing tumor. Histopathological evaluation confirmed a glioblastoma multiforme (WHO °IV). The MRI images indicate the exact location of tissue sampling. *Sample a* was taken from the strong contrast enhancing tumor center, *sample b* from a less enhancing tumor region, *sample c* from the transition zone to the low-grade tumor region, and *sample d* from the surrounding hypointense area in the T1-weighted MRI images beyond the main tumor border. IR spectroscopic classification of the tumor specimens assigned *sample a* to glioma WHO°IV with some hemorrhage and other tissue. The majority of *sample b* was assigned to glioma WHO°III with smaller fractions of glioma WHO°IV, glioma WHO°II, hemorrhage, and other tissue. *Sample c* was predominantly assigned to glioma WHO°II with some glioma WHO°III. *Sample d* was almost completely assigned to normal brain tissue. All assignments agree well with the histopathological evaluation of the four specimens.

Figure 2 shows the results from IR spectroscopic tissue classification of ten specimens from patient 6 with a multifocal glioblastoma. In the course of the neurosurgical resection of the two contrast-enhancing tumors multiple tissue specimens were taken from both tumor centers and from the surrounding edema zone using neuronavigational

Table 2 Main criteria for assessment of malignancy grade according to neuroradiological, IR spectroscopic, and histopathological findings

Grade ^a	MRI		IR Spectroscopy		Histology	
	Signal properties	Localization	Predominant tissue category	Highest tissue category	Predominant cell density	Maximal cell density
NT	Normal T1/ T2 edema	Surrounding edema zone	Normal tissue (green)		Regular cell density	Normal tissue
°2	Hypointense T1/ no contrast enhancement	Low-grade tumor zone	Glioma°II (blue)		Low tumor cell density	Glioma °II
°3	T1 with contrast enhancement without necrosis	Low-grade /high-grade transition zone	Glioma°III (orange)		Intermediate tumor cell density	Glioma °III
°4	T1 with contrast enhancement and necrosis	High grade tumor center	Glioma°IV (red)		High tumor cell density	Glioma °IV

^a Grade of malignancy
NT: normal tissue

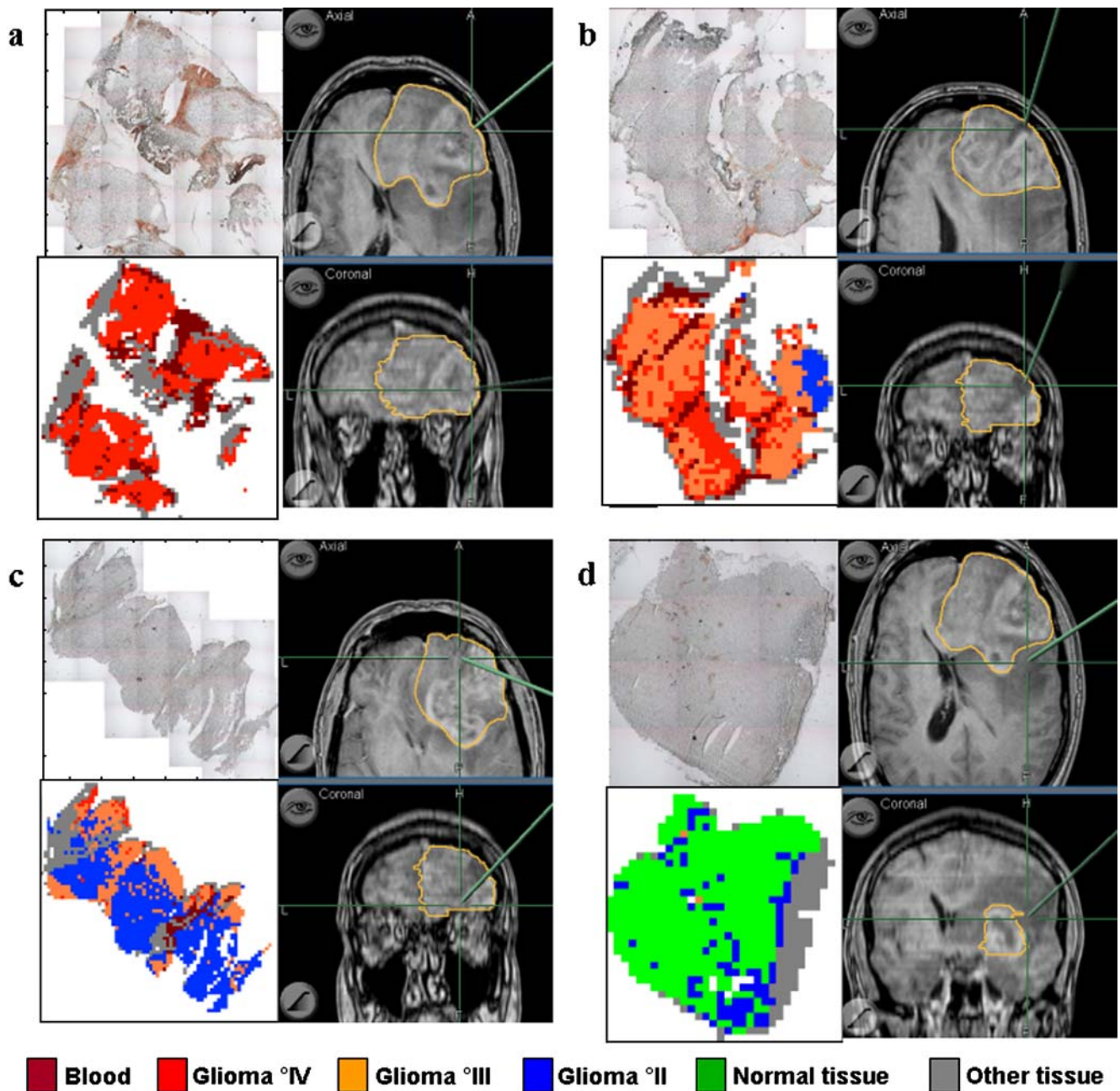


Fig. 1 Four out of twelve specimens from patient 2 with a right frontal glioblastoma multiforme (WHO°IV). Photographs of the unstained cryosections (*top left*) and color-coded tissue classification based on FTIR images (*bottom left*). Axial and coronal MRI-T1-

weighted images (*right*) after administration of gadolinium demonstrate the exact location of specimen sampling in the 3D data set of the neuronavigation

guidance. The exact locations of the sampling are visualized on the neuronavigational MRI scan in Fig. 2. Samples 3, 4, 8, 9, and 10 were taken from the contrast-enhancing tumors and IR spectroscopic analysis predominantly classified the specimens as high-grade glioma tissue (WHO °III/°IV). Samples 6 and 7 directly surrounding the anterior high-grade tumor nodule were classified to low-grade glioma tissue (WHO°II). Specimens 1, 2, and 5 were obtained from the dorsal tumor side, approximately 2 cm from the contrast

enhancing tumor nodule. The IR spectroscopic images of the tissue specimens contained a significant amount of normal tissue in addition to a low-grade tumor portion in samples 1 and 2 and completely normal brain tissue in sample 5. Again the IR spectroscopic classification was in excellent agreement with independently performed histopathological evaluation of the specimens.

Figure 3 shows FTIR images from all 54 tissue sections of six glioma patients. FTIR images four and five of patient 1,

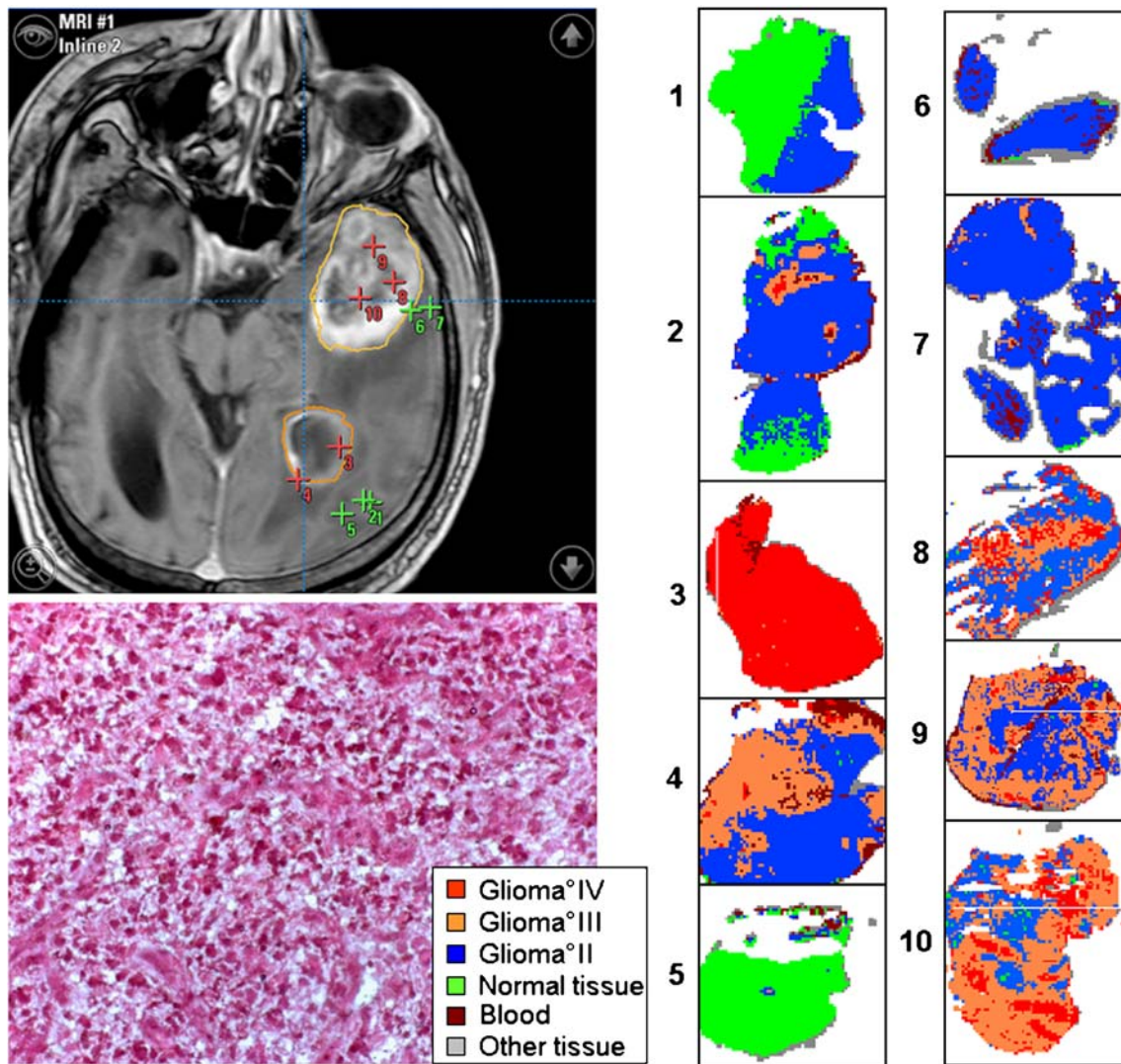


Fig. 2 Patient 6 with a multifocal glioblastoma multiforme: two contrast enhancing tumors right temporopolar and right temporooccipital. Localization of the tissue sampling on MRI scan of the neuronavigation (*top left*). H&E-stained tissue section of sample 3

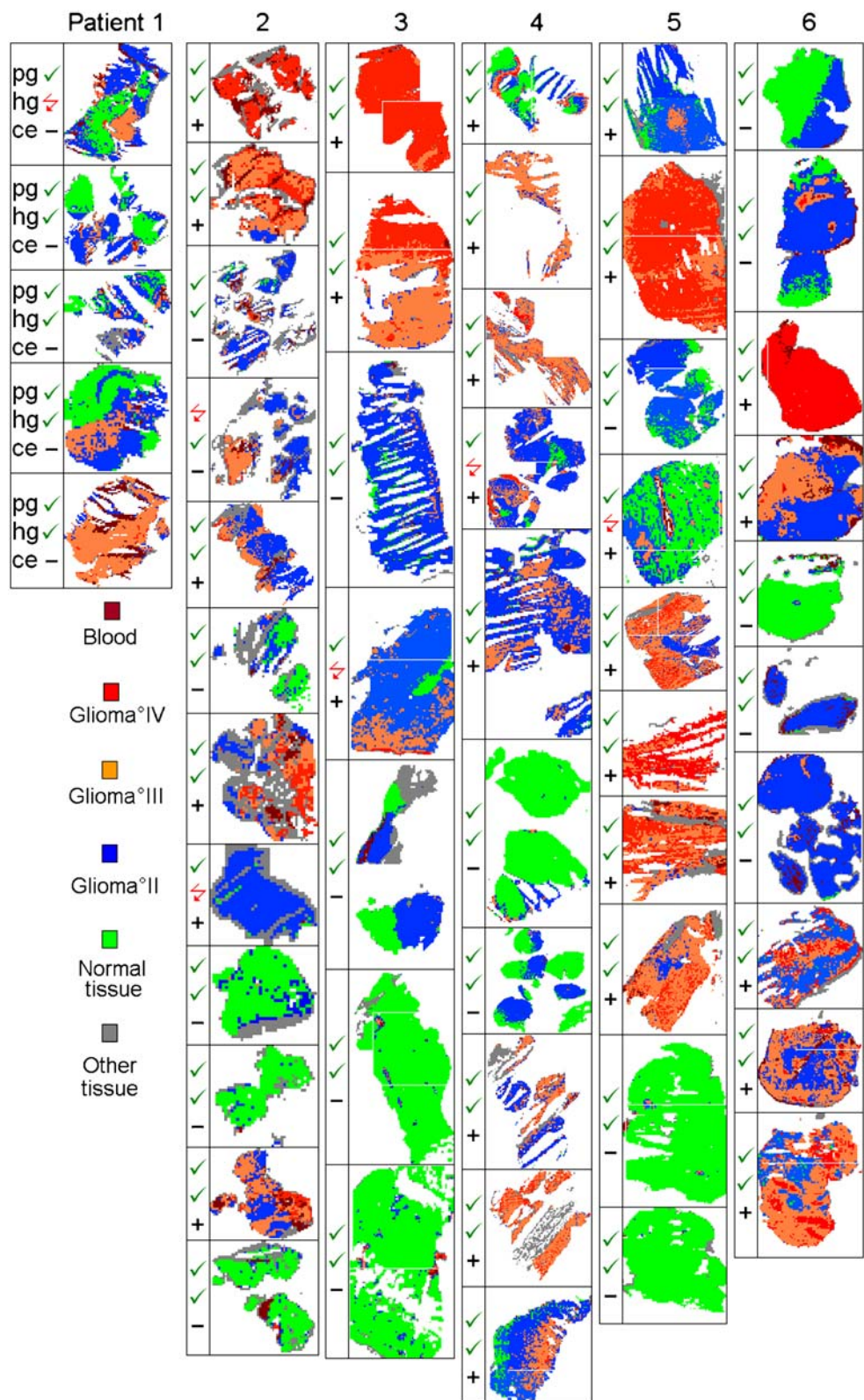
demonstrates the typical appearance of glioblastoma multiforme (*bottom left*). FTIR images of the ten unstained tissue sections. Colors represent classification by the LDA model

one and four of patient 2, one, four, and six of patient 3, and the underlying IR spectra have already been presented in previous manuscripts [20, 21]. The classification results in Fig. 3 slightly deviate from the previous results because the baseline-correction procedure of the training data and, consequently, the LDA model were modified in the meantime. In each patient, high-grade and low-grade tumor and normal tissue could be reliably differentiated. Whereas specimens resected from homogeneous areas according to MRI usually resulted in homogeneous patterns in the IR spectroscopic classification images, specimens from the tumor borders such as the transition zone from low-grade to high-grade areas and to normal brain tissue typically contained regions of adjacent tissue types in the spectroscopic classification images. In summary, the results

demonstrate that more than one tissue class or tumor grade might be present in each specimen which complicates comparison of histopathology and IR spectroscopy.

Tissue sections were evaluated in accordance with the most unfavorable findings, which is equivalent to the highest grade, and to the predominant tumor type. Agreement or the disagreement of the IR-based classification with both criteria according to the gold standard histopathology is indicated in Fig. 3 by green ticks or red flashes. Positive or negative contrast enhancement on MRI is indicated by plus or minus signs. It is interesting to note that sample 5 of patient 1 was correctly assigned to tumor grade °3 by IR spectroscopy and histopathology although the tumor showed no contrast enhancement on MRI. Table 3 summarizes the results applying both criteria. From 29 tumor

Fig. 3 Overview of FTIR images of all 54 tissue specimens of the six glioma patients (Table 1). Colors represent classification by the LDA model. Agreement or disagreement of the IR-based classification with the predominant grade (*pg*) and highest grade (*hg*) according to the gold standard histopathology is indicated with a *green tick* or *red flash*. Positive or negative contrast enhancement (*ce*) is indicated by *plus* or *minus* symbols



samples that were assigned to high-grade tumor tissue on the basis of the most unfavorable findings in the histological evaluation, 22 samples showed a predominantly homogenous high-grade and seven a predominantly low-

grade classification pattern. The spectroscopic analysis also recognized in five of the seven predominantly low-grade cases single regions representing high-grade tumor areas. From the remaining 25 samples representing low-grade

Table 3 IR spectroscopic detection of malignant glioma portion (°III and °IV) according to the predominant grade in the specimen and according to the highest grade

IR spectroscopy	Histology:		Sum
	WHO°III/°IV	NT/WHO°II	
<i>Predominant grade in the specimen</i>			
Grade III/IV	22	1	23
NT/Grade II	0	31	31
Sum	22	32	54
<i>Highest grade</i>			
Grade III/IV	27	3	30
NT/Grad II	2	22	24
Sum	29	25	54

NT: normal tissue

tumor or almost normal brain tissue in the histological examination, three specimens showed regions of a high-grade tumor tissue category whereas 22 were consistently assigned to the low-grade categories by spectroscopy. Altogether, on the basis of the highest tumor grade of a tissue sample in the histological evaluation, the average sensitivity and specificity of the spectroscopic analysis of high-grade tumor were 93.1% and 88.0%, respectively (Table 4). Considering the predominant tumor cell density in the histological evaluation, all of 22 high-grade tumor specimens and 31 out of 32 low-grade tumor specimens were consistently categorized to high-grade and low-grade tumor tissue, respectively, in the spectroscopic evaluation. This results in improved sensitivity of 100% and a specificity of 96.6% that were included in Table 4.

Discussion

The objective of neurosurgical treatment of high-grade glioma is to remove the contrast-enhancing tumor nodules representing the high-grade portion of a malignant glioma. In this part of the tumor there is no residual functional brain and resection does not cause neurological worsening of the patients' condition. Low-grade-tumor regions, however, may still be functional and in the case of an eloquent brain area may not be removed because of a resulting neurological deficit. Prognosis of the patient depends on the amount of residual high-grade tumor that will determine the probability and time until local recurrent tumor will occur in the patient [7]. Therefore, identification of the high-grade portion is crucial to improving surgical treatment of malignant glioma. In this study tissue specimens that were resected under preoperative MRI-based neuronavigation surveillance were classified using IR spectroscopic imaging and the results were compared with those from histopathologic evaluation as the gold standard.

According to the WHO classification standards, histological diagnosis is based on the most unfavorable findings within the tumor tissue that is subjected to histopathology. These findings determine the highest tumor grade. For intraoperative evaluation of resectability of the tumor borders the predominant tissue type in a two-class system may be more informative. The combined classes normal tissue/low tumor grade and tumor grades °3/°4 are the most relevant for the neurosurgeon to decide intraoperatively whether or not to extend the current resection of the tumor. Tissue regions of non-predominant high tumor grade are usually retained in order to minimize the risk to the patient of neurological deficits. Residual high-grade tumor in the transition zone is often hard to identify but may significantly influence the prognosis of patients. Therefore, the most important objective is to determine tissue regions of predominantly high-grade tumor. The results in Table 4 revealed that this can be achieved almost perfectly by using IR spectroscopy. Determination of the predominant tumor grade by IR spectroscopy is slightly more accurate in terms of sensitivity and specificity than determination of the highest grade. Histopathologic determination of the highest tumor grade seems to be more accurate if the malignant tumor portion is not predominant. This might be because light microscopic evaluation of stained tissue sections offers higher optical resolution and enables detection of smaller tumor regions. Furthermore, histopathologic evaluation considers more features for grading than the cellularity and the correlated biochemical composition which are probed by IR spectroscopy. Classification of gliomas is not trivial, because gliomas are highly diverse and the grades form a histological continuum. Histopathologic criteria also include nuclear pleomorphism, mitotic activity, endothelial proliferation, and necrosis [22, 23]. For example, a single tumor sample may encompass regions of different grades of malignancy. Furthermore, the assignment of °IV does not only depend on cellularity and malignant morphology but also on criteria such as necrosis and/or endothelial proliferation. However, these criteria are crucial to the diagnosis and thus the planning of postoperative therapy. In summary, whereas a two-class classification model offers appropriate information for the neurosurgeon, a multi-class model and higher laterally resolved FTIR images are expected to improve agreement with the gold standard

Table 4 Sensitivity and specificity of IR spectroscopic detection in comparison with histopathology according to the predominant and highest grades

IR spectroscopy	Histology:	
	Predominant grade	Highest grade
Sensitivity	100% (22/22)	93.1% (27/29)
Specificity	96.9% (31/32)	88.0% (22/25)

histopathology. Beside this, one of the long-term goals of IR spectroscopy is to obtain tissue information on a molecular level which could be used to plan an optimized therapy. This objective would also benefit from a more differentiating system.

Conclusions

In this study we evaluated the suitability of IR spectroscopic imaging for determining the malignancy grade of intraoperatively collected tumor specimens. Snap-frozen tissue sections were prepared and their spectroscopic grading was obtained by use of multivariate feature extraction and classification methods. The results were compared with histopathological findings of consecutive frozen sections of the biopsy samples and the neuroradiological characteristics of the location of the biopsy using neuronavigational guidance. The high success rate demonstrated that IR spectroscopic imaging can provide the neurosurgeon and histopathologist with a new rapid tool for detecting and grading brain tumors. This technique might be useful not only in the pathology laboratory but also in the operating theater as an on-site means of identifying tumor margins.

Realization of the IR spectroscopic imaging approach in a clinical setting requires:

1. preparation of tissue sections on IR-transparent substrates using a cryotome;
2. installation of a spectrometer system near the operating room; and
3. trained medical personal to operate the instruments.

The latest generation of FTIR imaging spectrometer is technically sophisticated, user friendly, and enables acquisition of an FTIR image in less than one minute. The algorithms for data analysis and classification will be integrated into a graphics user interface in the near future. The cost of an FTIR imaging system is still above 100,000 EUR. However, further clinical applications are expected for tissue classification by FTIR imaging once the advantages of the technique have become known by the medical community.

Clinical validation of the concept requires long-term statistics of the patients' life expectation; this is, however, beyond the scope of this paper. Although this general approach has been illustrated here for classifying and grading primary tumors of the glioma type, the same method is expected to complement established methods in other biomedical and diagnostic applications. Other fields include

evaluation of biological tumor activity, which could be used for more precise planning of postoperative therapy, or classification of other tumor entities, e.g. brain metastases [15, 16], prostate carcinoma [24] or breast lesions.

References

1. Chamberlain M, Kormanik P (1998) *West J Med* 168:114–120
2. Hess K (1999) *J Neurooncol* 42:227–231
3. Lacroix M, Abi-Said D, Fourney DR, Gokaslan ZL, Shi W, DeMonte F, Lang FF, McCutcheon IE, Hassenbusch SJ, Holland E, Hess K, Michael C, Miller D, Sawaya R (1999) *J Neurosurg* 95:190–198
4. Shapiro W, Shapiro J (1998) *Oncology (Huntingt)* 12:233–240
5. Toms S, Ferson D, Sawaya R (1999) *J Neurooncol* 42:215–226
6. Wisoff J, Boyett J, Berger M, Brant C, Li H, Yates A, McGuire-Cullen P, Turski P, Sutton L, Allen J, Packer R, Finlay J (1998) *J Neurosurg* 89:52–59
7. Stummer W, Pichlmeier U, Meinel T, Wiestler OD, Zanella F, Reulen HJ (2006) *Lancet Oncol* 7(5):392–401
8. Willems PWA, Taphoorn MJB, Burger H, Berkelbach van der Sprenkel JW, Tulleken CA (2006) *J Neurosurg* 104:360–368
9. Bohinski RJ, Kokkino AK, Warnick RE, Gaskill-Shipley MF, Kormos DW, Lukin RR, Tew JM (2001) *Neurosurgery* 48:731–742
10. Wirtz CR, Albert FK, Schwaderer M, Heuer C, Staubert A, Tronnier VM, Knauth M, Kunze S (2000) *Neurol Res* 22:354–360
11. Krafft C, Salzer R (2008) In: Diem M, Chalmers JM, Griffiths PR (eds) *Vibrational spectroscopy for medical diagnosis*. Wiley, Chichester
12. Krafft C, Sobottka SB, Schackert G, Salzer R (2004) *Analyst* 129:921–925
13. Steiner G, Shaw A, Choo-Smith LP, Abuid MH, Schackert G, Sobottka SB, Steller W, Salzer R, Mantsch HH (2003) *Biopolymers* 72:464–471
14. Beleites C, Steiner G, Sowa MG, Baumgartner R, Sobottka S, Schackert G, Salzer R (2005) *Vib Spectrosc* 38:143–149
15. Krafft C, Shapoval L, Sobottka SB, Schackert G, Salzer R (2006) *Technol Cancer Res Treat* 5:291–298
16. Krafft C, Shapoval L, Sobottka SB, Geiger KD, Schackert G, Salzer R (2006) *Biochim Biophys Acta* 1758:883–891
17. Krafft C, Sobottka SB, Schackert G, Salzer R (2006) *J Raman Spectrosc* 37:367–375
18. Krafft C, Sobottka SB, Schackert G, Salzer R (2005) *Analyst* 130:1070–1077
19. Krafft C, Kirsch M, Beleites C, Schackert G, Salzer R (2007) *Anal Bioanal Chem* 389:1133–1142
20. Krafft C, Thümmel K, Sobottka SB, Schackert G, Salzer R (2006) *Biopolymers* 82:301–305
21. Krafft C, Sobottka SB, Geiger KD, Schackert G, Salzer R (2007) *Anal Bioanal Chem* 387:1669–1677
22. Kleihues P, Soylemezoglu F, Schauble B, Scheithauer BW, Burger PC (1995) *Glia* 15:211–221
23. Louis DN, Holland EC, Cairncross JG (2001) *Am J Pathol* 159:779–786
24. Bhargava R, Fernandez DC, Hewitt SM, Levin IW (2006) *Biochim Biophys Acta* 1758:830–845